NUMERICAL SIMULATION OF HYDRODYNAMIC WAVE LOADING BY A COMPRESSIBLE TWO-PHASE MODEL

R. Wemmenhove[*], G.E. Loots and A.E.P. Veldman

[*]University of Groningen, Department of Mathematics
P.O. Box 800, 9700 AV, The Netherlands
e-mail: r.wemmenhove@math.rug.nl

Key words: Wave loading, Two-phase flow, Numerical simulation, Volume-of-Fluid, Compressibility

Abstract. *The numerical simulation of hydrodynamic wave loading on different types of offshore structures is important to predict forces on and water motion around these structures. This paper presents a numerical study of the effects of two-phase flow on an offshore structure subject to breaking waves. The numerical model, an improved Volume Of Fluid (iVOF) method, has been developed initially as a one-phase model to study the sloshing of liquid fuel in satellites. In the one-phase approach, the method solves the incompressible Navier-Stokes equations with a free-surface condition on the free boundary. The discretisation of the equations is done on a staggered grid, using an explicit first order Forward Euler Method. The model has been extended recently to take two-phase flow effects into account. In the incompressible two-phase model the VOF-function is used to determine the aggregated density value inside a grid cell. Rapid changes in density in grid cells, up to a factor 1000, impose a challenge with respect to numerical stability. However, by using a newly-developed gravity-consistent discretisation, spurious velocities at the free surface are prevented. Thus far, the second phase has been treated as incompressible. Taking compressibility into account makes it possible to simulate in particular the behaviour of the air phase more realistic. As the condition of incompressibility no longer holds for gaseous grid cells, an equation of state is required as the third main equation. The calculation of pressure and density values now occurs simultaneously due to this equation of state, while the expansion and compression of air pockets are considered as an adiabatic process. The numerical model has been validated on several test cases. In this paper special attention is paid to both the validation on a simple test case (falling drop) and the validation of wave loading on a fixed offshore structure.*

1 INTRODUCTION

Hydrodynamic wave loading is a major research issue in offshore environments. During violent weather conditions offshore structures are subject to different types of wave

impact. The impacting waves are complex mixtures of water and air, the properties of the mixture having a serious effect on velocity fields around and presure levels on offshore structures. During wave impact on vertical walls, there is experimental evidence [1] that peak pressure levels decrease due to the presence of air in the water, however the duration of the wave impact may increase. The two-phase flow effects mainly occur in the vicinity of the free surface, where the components air and water are mixed as air pockets, bubbles and spray. Spray is of minor relevance for determining pressure loads, as these water drops induce minor pressure loads on offshore structures. Air pockets and bubbles, however, can seriously affect hydrodynamic forces. Air pockets are relatively large, with a diameter up to $O(10^2)mm$, and they have a short lifetime during wave impact. Just after wave impact, they quickly defragment into smaller entities [3]. Air bubbles, on the other side, have a typical diameter of $O(10^0)mm$. This imposes a difficulty to track these small entities individually, as the typical grid dimensions are much larger.

Simulations of hydrodynamic wave loading occur mainly by one-phase models, considering only the water phase. Most models focus on specific aspects of free surface flows, such as wave impact of aerated flow (water mixed with many small air bubbles) on walls or the velocity field under breaking waves.

As soon as flow conditions are getting more violent, using a two-phase flow model is strongly recommendable. However, the small spatial and temporal scales of the air pockets and bubbles are a serious problem. Typical spatial scales in offshore domains are of the order of hundreds of meters, while air pockets rarely have diameters of 1 meter. So, keeping track of the air phase in large-scale offshore problem is a challenging task, even when using powerful computers.

Existing two-phase models focus either on single bubbles or on quite regular waves. Scardovelli [13] gives a nice overview of existing two-phase flow models. However, there has been much progress in the simulation of two-phase flow in recent years.

The VOF algorithm [9] is used as basis for the displacement of the interface. The advantages of the VOF algoritm are its good mass conservation properties and its ability to simulate the break-up and merging of the free surface. Other interface displacement methods, like the level-set method, have more problems with mass conservation and have difficulties to handle complex free surface shapes [10]. The VOF algorithm is combined with a local height function to improve the shape of the free surface and to prevent form floatsam and jetsam [11]. The local height function, originally proposed by [6], is now used more widely [4].

Inconsistent modeling of the free surface can lead to unphysical spurious velocities. These spurious velocities are addressed to different reasons [2],[15],[16], but in this paper we propose an approach to prevent from spurious velocities in at least the steady hydrostatic case.

To improve the modeling of the air phase, in particular in regions with entrapped air,

compressibility of the air is taken into account. To model air compressibility, the ideal gas law [5],[14], the adiabatic relationship [7],[8] and the speed of sound [10] are options for the equation of state in the absence of temperature effects. In this paper the adiabatic relationship is used as the equation of state for the gaseous parts of the grid.

The next section of this paper describes the details of the numerical model. Aside from the governing equations and the improved Volume Of Fluid (iVOF) method, particular attention is paid to a proper representation of the free surface. By using a correct density treatment, spurious velocities at the free surface are prevented. Subsequently the compressibility of the air is described.

A key aspect of the present model is the validation on suitable test cases. Before showing the validation on a real measurement, the model is tested on a straightforward case: a falling water drop in one dimension. After that, the results of a simulation with wave impact on an offshore structure are presented and discussed.

2 Numerical model

For each point in the domain the fluid motion is governed by the continuity equation and the momentum equation:

$$\frac{\partial \rho}{\partial t} + \nabla \cdot (\rho \mathbf{u}) = 0 \qquad (1)$$

$$\frac{\partial (\rho \mathbf{u})}{\partial t} + \underbrace{\nabla \cdot (\rho \mathbf{u}\mathbf{u})}_{convection} + \nabla p + \underbrace{\nabla \cdot (\mu \nabla \mathbf{u})}_{diffusion} + \rho \mathbf{F} = 0 \qquad (2)$$

with $\mathbf{F}$ an external body force like gravity, velocity $\mathbf{u}$, pressure p, density ρ and dynamical viscosity μ.

For incompressible flow, the velocity field is divergence-free, reducing the continuity equation to

$$\nabla \cdot \mathbf{u} = 0 \qquad (3)$$

The continuity equation and momentum equation are, after semi-discretisation in time, combined to the pressure Poisson equation to compute the new pressure value and velocity field. This pressure equation is shown in section 2.2.

2.1 iVOF algorithm

The advection of water and air in the current model is based on the Volume Of Fluid (VOF) algorithm as developed by Hirt and Nichols [9].

As long as a one-phase approach was used for the model, the incompressible Navier-Stokes equations were solved with a free-surface condition on the free boundary. The VOF function F_s (with values between 0 and 1) determined whether or not the flow field in a grid cell was calculated.

This is in contrast with the two-phase approach, where the air-water interface is no longer considered as a free surface, although the interface is still reconstructed using the VOF algorithm. Numerically important is now the density jump across the air-water interface, as the density can increase or decrease a factor 1000, imposing a challenge to the numerical stability of the model. The liquid fraction F_s is now used to calculate the aggregated density in a grid cell, this occurs by weighted averaging:

$$\rho = F_s\rho_l + (1 - F_s)\rho_g \tag{4}$$

with ρ_l the liquid density and ρ_g the density of the gas.

The numerical model has been implemented in a 3D VOF Navier-Stokes solver called COMFLOW. Compared with the original VOF algorithm, a local height function improves the treatment of the free surface [6]. The program COMFLOW has been developed initially by the University of Groningen to study the sloshing of liquid fuel in satellites [6]. This micro-gravity environment requires a very accurate and robust description of the free surface. In close cooperation with MARIN (Maritime Research Institute Netherlands), this methodology was later extended to the calculation of green water loading on a fixed bow deck and to other offshore problems [11].

2.2 Discretisation

The discretisation of the Navier-Stokes equations is done on a staggered Cartesian grid, which means that the pressure and the density are set in the cell centres and the velocity components in the middle of the cell faces between two grid cells. The discretisation occurs by a first-order upwind scheme. The numerical dissipation inherent to this scheme can be regarded as some kind of turbulent dissipation.

For **incompressible** flow conditions, the Navier-Stokes equations, as given by eq.(1) and eq.(2), are discretised in time according to the explicit first order Forward Euler method:

$$\nabla \cdot \mathbf{u}^{n+1} = 0 \tag{5}$$

$$\frac{\mathbf{u}^{n+1} - \mathbf{u}^n}{dt} + \nabla \cdot (\mathbf{u}\mathbf{u})^n + \frac{1}{\rho^n}\nabla p^{n+1}$$

$$+ \frac{1}{\rho^n}\nabla(\mu^n\nabla\mathbf{u}^n) + \mathbf{F}^n = 0 \tag{6}$$

with n the old time level and $n + 1$ the new time level. Notice that ρ^n can vary due to the variation of the liquid fraction in a grid cell, although the flow is incompressible.

Now, the divergence of the momentum equation is taken. The term $\nabla \cdot \mathbf{u}^{n+1}$ is isolated and inserted in the momentum equation. This results in the pressure Poisson equation:

$$\nabla \cdot (\frac{1}{\rho^n}\nabla p^{n+1}) = \frac{1}{dt}(\nabla \cdot \mathbf{u}^n) - \nabla^2(\mathbf{u}^n\mathbf{u}^n) - \nabla(\frac{1}{\rho^n}\nabla(\mu^n\nabla\mathbf{u}^n)) - \nabla \cdot \mathbf{F}^n \tag{7}$$

After this equation has been solved for the pressure, the new velocity field u^{n+1} is found by inserting this new pressure field in the momentum equation (6). The discretisation of the compressible equations follows in section 2.4.

2.3   Density calculation at the interface

Special attention should be given to the discretisation of the density. Like the pressure, the density is a scalar variable, originally located at the center of a grid cell. Physically, it has only two values: the density of water and the density of air.

According to the solution method, the velocity field at the new time level is acquired by adding a term to the old velocity field (see equation (6)). Since the velocity field is highly continuous between the old and new time level, this term, $\nabla p/\rho$, should also be smooth. Since the pressures are located in cell centres, the term ∇p has to be calculated in a control volume located between two cell centers. The density value ρ should hold – and be defined properly – in the control volume located which is located between the cell centres.

Consider the situation in figure 1. The free surface dividing water (below) and air (above) is in this case a straight line with a slope of $\frac{1}{2}$. We need for both the horizontal and vertical direction a proper discretisation of the term $\nabla p/\rho$. The suggested control volumes for these terms are depicted with dashed lines, between cells A and F (vertical), and E and A (horizontal). As the pressure values are registrated at the circles, the discretization can be straightforward: $\frac{1}{\rho}\frac{\partial p}{\partial x}\mid_{EA}\approx \frac{1}{h_x}\frac{(P_A-P_E)}{\rho_{EA}}$. Near the free surface, however, the density averaging is not clear beforehand. Consider for example the density ρ_{AB} in the control volume between A and B. Choices like 1 ("cell centres A and B both in air"), 125.875 ("average of complete cells A and B") or even 63.4375 ("average of right half of cell A and left half of cell B") can be defended.

Does it matter? In fact, quite a lot. Consider the situation above, and make it stationary by setting the gravity vector $\boldsymbol{g} = (g_x, g_z)^T = (5, -10)^T$. In that case, with all time derivatives and velocities zero, the momentum equations (2) are reduced to

$$\frac{\partial p}{\partial x} = \rho_x g_x, \qquad \frac{\partial p}{\partial z} = \rho_z g_z$$

Concentrating on the four cells A,B,C and D, we take the simple approach of defining the densities between the cells as the average of the weighted cell averages. So cell averages are approximately $\rho_A = 1, \quad \rho_B = 250, \quad \rho_C = 750$ and $\rho_D = 1000$. Further we suppose the cells have unit size.

Integrating the pressure in clockwise direction from A to D (via B) gives

$$\begin{aligned} P_D = P_B - h_z g_z \rho_{BD} &= P_A + h_x g_x \rho_{AB} - h_z g_z \rho_{BD} \\ &= P_A + 5 \cdot 125 + 10 \cdot 625 = P_A + 6875, \end{aligned} \tag{8}$$

while integrating in counterclockwise direction (from A to D via C) gives

$$P_D = P_C + h_x g_x \rho_{CD} = P_A - h_z g_z \rho_{AC} + h_x g_x \rho_{CD}$$

$$= P_A + 10 \cdot 375 + 5 \cdot 875 = P_A + 8125. \tag{9}$$

This inconsistency (the contour integral not being zero) is immediately visible numerically: spurious velocities will occur around the free surface, see figure 3. So a more consistent density discretisation, which at least will cope correctly with stationary situations, is needed. It requires the gravitational force $\rho \mathbf{g}$ to be conservative.

This very simple skewed-gravity example, however, provides a strategy for such a gravity-consistent discretisation. The pressure is known analytically: hydrostatic and 'aerostatic' in both phases, respectively. If we choose $p = 0$ at the free surface then (see figure 2):
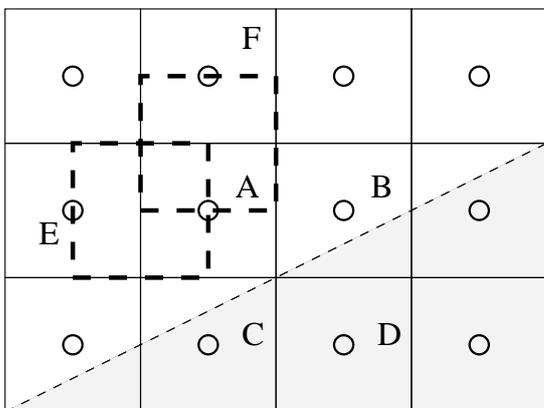
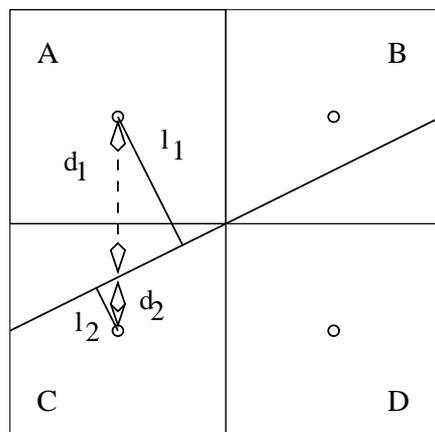Figure 1: *Averaging of density. The cells are numbered according to their position in the flow field.*

Figure 2: *Gravity-consistent discretisation*

$P_A = -l_1 \rho_1 \mid \mathbf{g} \mid = d_1 \cos \alpha \frac{g_z}{\cos \alpha} = d_1 \rho_1 g_z$ where α is the slope angle, and
$P_C = l_2 \rho_2 \mid \mathbf{g} \mid = -d_2 \rho_2 g_z$.

Together with $\frac{1}{\rho_z} \frac{\partial p}{\partial z} = g_z$, this gives

$$\rho_{AC} = \frac{1}{g_z} \frac{P_A - P_C}{d_1 + d_2} = \frac{d_1 \rho_1 + d_2 \rho_2}{d_1 + d_2}. \tag{10}$$

A similar construction gives simply $\rho_{AB} = \rho_1$, because both cell centres are in the fluid with density ρ_1. Using the local height function also used in the iVOF algorithm, the distances d_1 and d_2 can easily be computed.

In the given example, this leads to $\rho_{AB} = 1, \rho_{AC} \approx 250, \rho_{BD} \approx 750$ and $\rho_{CD} = 1000$, which gives a consistent density field and no spurious velocities.

Note that in this approach, the cell pressure was in some sense indentified with the pressure in the centre of the cell. This leads to the possibility of other ways of averaging the density, besides this 'cell-centered'-approach. Some of them are still under investigation.
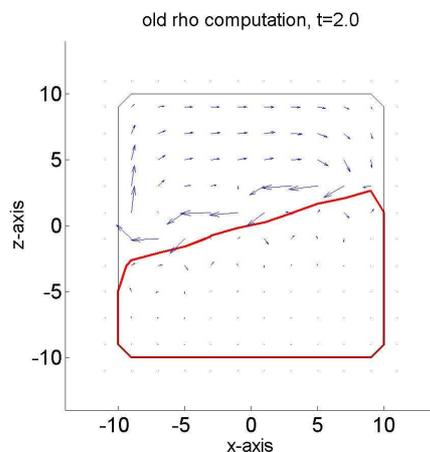
Figure 3: *Spurious velocities due to simple averaging of density*

2.4 Including air compressibility

For compressible flow, the divergence-free condition of the velocity field, $\nabla \cdot \mathbf{u} = 0$, no longer holds, so we keep the semi-discretised form of the continuity equation (1):

$$\frac{\rho^{n+1} - \rho^n}{dt} + \mathbf{u}^n \nabla \rho^n + \rho^n \nabla \cdot \mathbf{u}^{n+1} = 0 \tag{11}$$

This equation is divided by the density and the term $\nabla \cdot \mathbf{u}^{n+1}$ is substituted again by the divergence of the momentum equation. The acquired Poisson equation is similar to equation (7), but with two extra terms:

$$\nabla \cdot (\frac{1}{\rho^n} \nabla p^{n+1}) = \frac{1}{dt\,\rho^n} \frac{\rho^{n+1} - \rho^n}{dt} + \frac{1}{dt} \frac{\mathbf{u}^n}{\rho^n} \nabla \rho^n +$$
$$\frac{1}{dt}(\nabla \cdot \mathbf{u}^n) - \nabla^2(\mathbf{u}^n \mathbf{u}^n) - \nabla(\frac{1}{\rho^n} \nabla(\mu^n \nabla u^n)) - \nabla \cdot F^n \tag{12}$$

These extra terms are numerically dangerous because of the spatial and temporal derivatives of the density; at the free surface, the density can jump from 1 to 1000. However, we can split the density in an incompressible liquid part ρ_l and a compressible gas part ρ_g. Using the VOF function F_s, the cell density ρ is given by $F_s \rho_l + (1 - F_s)\rho_g$. Using $\frac{DF_s}{Dt} = 0$, the derivatives in equation (12) of the liquid part of the density appear to be equal to zero.
The remaining derivatives of the gas densities do not contain large jumps, as these derivatives are only determined by the compression and expansion of the gas phase. By the split up of the density into a liquid and gas part, the pressure Poisson equation (12) reduces

7

to

$$\nabla \cdot (\frac{1}{\rho^n} \nabla p^{n+1}) = +\frac{(1 - F_s^n)}{dt \, \rho^n} \frac{\rho_g^{n+1} - \rho_g^n}{dt} + \frac{(1 - F_s^n)}{dt} \frac{\mathbf{u}^n}{\rho_g^n} \nabla \rho^n +$$

$$\frac{1}{dt}(\nabla \cdot \mathbf{u}^n) - \nabla^2(\mathbf{u}^n \mathbf{u}^n) - \nabla(\frac{1}{\rho^n} \nabla(\mu^n \nabla \mathbf{u}^n)) - \nabla \cdot F^n \qquad (13)$$

The gas density at the new time level can be calculated by using the adiabatic pressure-density relation

$$\frac{p^{n+1}}{p_0} = (\frac{\rho^{n+1}}{\rho_0})^\gamma, \qquad (14)$$

with p_0 and ρ_0 the reference pressure and density values.

The adiabatic coefficient γ has a value of 1.4 for pure air, while incompressibility is associated with an infinite value of the coefficient γ.

3 Model validation: test cases

In this section the model is validated on two test cases. In case of a 1D falling water mass, the simulation results can be compared with an analytical solution. For the second test case, the dambreak experiment, the results are compared with measurements.

3.1 1D theoretical test case: falling water mass

To give a simple example of compressible flow, consider the falling water mass as sketched in figure 4. This is essentially a 1D-situation, with gravity in vertical direction.
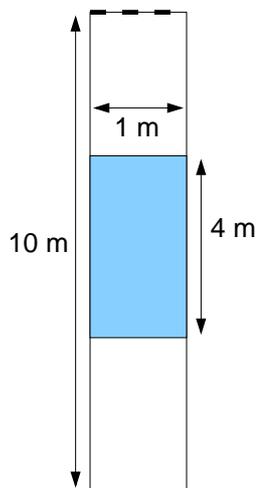

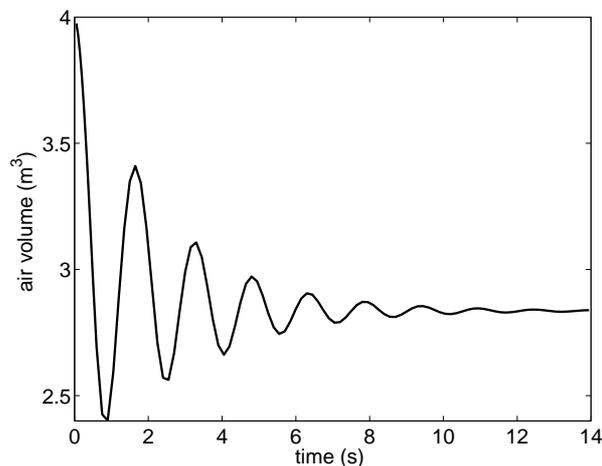Figure 4: *1D schematisation of a falling water mass*

Figure 5: *Pressure development in the air below a falling water mass for compressible flow*

It provides an easy example of the differences between the one-phase computational model and the incompressible and compressible two-phase models. The ceiling of the

8

column consists of an open boundary with Dirichlet condition $p = 0$. For the analytical solution, the pressure at the lower edge of the falling water mass is set equal to the pressure at the top side of the underlying air column. In the three cases, the following wil happen:

- **one-phase model**. The non-fluid part, i.e. the part which will be labeled with E-cells, is not modeled: no equations are solved there. In the F(luid) cells, the full Navier-Stokes equations involve the gravity term $\rho_{liq}g$. The liquid will freely accelerate downward (fall) without a pressure inside the fluid cells until the bottom is reached. At the time step when the lowest cell is filled, it will be labeled an F-cell, because of the construction described above. This involves mass conservation, so the liquid stops falling and the pressure will be hydrostatically distributed immediately. The pressure gradient now exactly counteracts the gravity force.

- **incompressible two-phase model** This model involves solving the incompressible Navier-Stokes equations in both phases. Because of the incompressibility, the air below the liquid cannot move and a static situation is attained immediately. The pressure now increases linearly from the ceiling ($p = 0$) with a small slope for the air, a large slope in the liquid part and again a small slope in the lower air part.

- **compressible two-phase model**. The air is now compressible. According to the adiabatic relationship $\rho_2 = \rho_1 \left(\frac{p_2}{p_1}\right)^{\frac{1}{\gamma}}$, the air volume V_{air} under the liquid column will decrease until the pressure difference of the air above and below the liquid compensates for the downward force gm_{fluid} while the relation $pV_{air}^{\gamma} = const$ remains valid. For example, with $\gamma = 1$, $m_{liq} = \rho_{liq}V_{liq} = 4000$, the pressure under the liquid will eventually be $140kPa$ with a volume of $\frac{100}{140}V_{air,0}$. According to the theoretical calculation, the trapped air column will show an oscillating behviour with a frequency of about $0.55Hz$. The actual simulation indeed shows this behaviour, with a final air volume of $2.8m^3$ and an oscillation frequency of $0.6Hz$ (see figure 5).

3.2 Complex test case: dambreak experiment

The two-phase numerical model has been tested on several offshore problems. One of the test cases is the dambreak simulation, which can be regarded as a simple model of green water flow on the deck of a ship. The numerical simulation is compared with model experiments performed at Maritime Research Institute Netherlands (MARIN). During the experiment measurements have been performed of water heights, pressures and forces on different locations. The small box in figure 6, which represents a container, is covered by eight pressure sensors, while the water height is measured at several locations behind and in front of the small box. Figure 6 shows snapshots of the model experiment and the numerical simulation in an early stage of the experiment, just before the water front reaches the left wall.

Regarding figure 6, there is a visual agreement between the snapshots of simulation and experiment. Of course, quantitative agreement is needed. Therefore, the water height
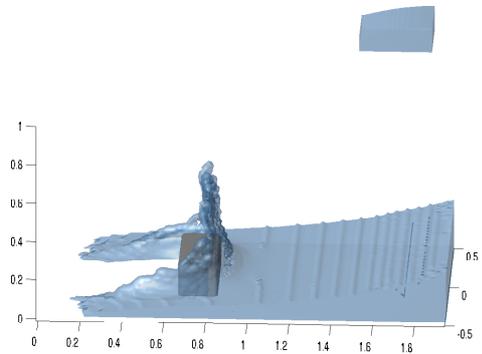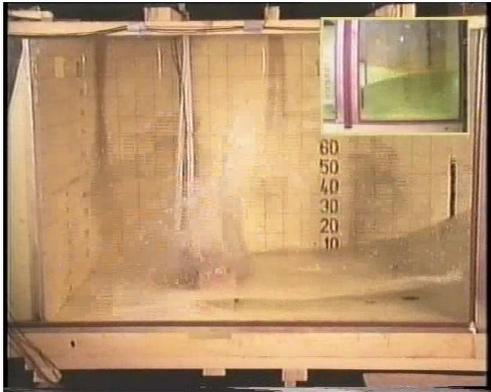
Figure 6: *Snapshots of dambreak experiment and simulation with a box in the flow, t = 0.56s*

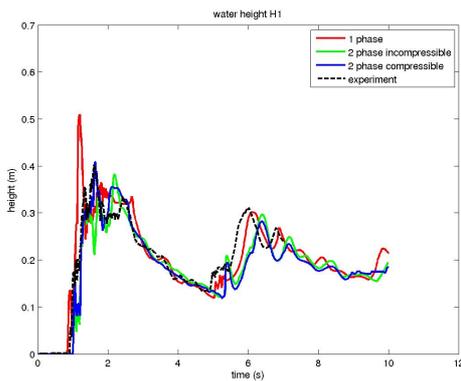just behind the box and the pressure level on the box are examined.

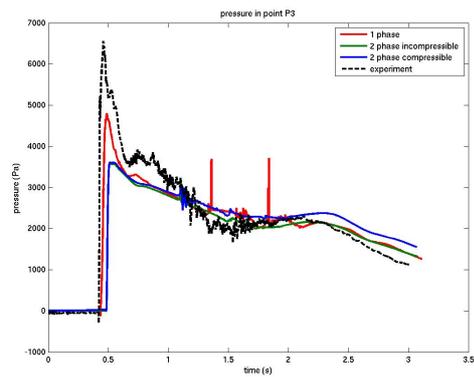Figure 7: *Water height development just behind (i.e. left of) the small box*

Figure 8: *Pressure development at the front (right edge) of the small box*

Figure 7 shows the water height development just behind the small box. The dashed line shows the water height for the experiment, while the solid lines shows the water height for the one-phase model, the incompressible two-phase model and the compressible two-phase model. The one-phase model predicts a water level at $t = 1s$ which is clearly too high, while the rise time is too short. The results of the experiment and the incompressible and compressible two-phase model show a large resemblance, although the water in the two-phase simulation reaches the measurement location slightly later. This may be caused by the treatment of the air viscosity in the model. Due to the upwind discretisation, artificial diffusion in the model changes the viscosity of the air to a value larger than the physical one. Therefore, the water needs a larger effort to push the air away, resulting in a slower advancement of the water front in the numerical model.

10

For the pressure level development (figure 3.2), the overall trend of measurement and numerical simulations is quite similiar. The initial pressure peak of the experiment is not correctly predicted by the one-phase simulation. The correlation between the (in-)compressible two-phase simulation and the experimental results is better. Furthermore, the one-phase simulation shows some artificial pressure spikes that are not present in the two-phase simulation. The pressure spikes in the one-phase model originate from the used cell labeling method. The cells containing just air (E-cells) are distinguished from the cells at the free surface (S-cells) and full water cells (F-cells). Due to the violent fluid motion, many topological changes may occur simultaneously within a single timestep in the numerical simulation. For the Empty and Surface cells in the one-phase model, mass conservation is not required by the numerical algorithm. Due to the rapid transition from Empty cells and Surface cells to Fluid cells, the pressure has to 'work' to achieve mass conservation in the newly created Fluid cells. This 'work' will manifest itself in a spike in the pressure signal of the one-phase model.

For the two-phase model, mass conservation is also applied to the Empty and Surface Cells. Mass conservation in all open cells prevents the model from giving pressure spikes as a result of changing cell labels. The result is a smoother pressure signal of the two-phase model.

Compared with other test cases in offshore environments, for example wave slamming, large air pockets are relatively insignificant for the dambreak problem. Due to the absence of large air pockets for this test case, compressibility of the air is of minor importance. However, for other test problems compressibility of the air has been proven to be important. For the shown test case of the falling drop, compressibility has been shown to be the major physical effect to let the water drop fall. For other large-scale validation cases, like sloshing in tanks [17] and overturning waves with slamming [12], compressibility is an important physical effect.

4 Conclusions and outlook

The hydrodynamics of different offshore applications can be simulated numerically using an iVOF Navier-Stokes solver. This paper shows the results of the extension of the numerical model to a two-phase model.

The main flow variables are now calculated in all grid cells. Furthermore, the density is now calculated at all locations. Particular attention has been paid to the calculation of the density at the free surface. By doing this such that the gravitational force becomes conservative, spurious velocities are prevented.

To improve the simulation of the dynamics of the air phase, compressibility has been introduced. The air phase is subject to adiabatic compression and expansion.

For different test cases, it has been shown earlier that the simulation results from the two-phase model correlate better with available measurement results [17] than the results from the one-phase model. The accuracy of the two-phase simulation increases when

compressibility of the air phase is taken into account. For the dambreak test case there is a minor improvement due to the air compressibility, but for other test cases, with a more pronounced air entrapment, the improvement is significant. As general applicability of the model for offshore problems is the main goal, the model will be validated on more test cases in future.

Acknowledgment

REFERENCES

[1] Bullock, G.N., Crawford, A.R., Henson, P.J., Walkden, M.J.A., Bird, P.A.D. The influence of air and scale on wave impact pressures. *Coastal Engineering*, **42**, 291-312, (2001).

[2] Coppola-Owen, H. and Codina, R. An improved level-set approach using finite elements with discontinuous gradient pressure shape functions. *Computational Methods in Marine Engineering*, Oslo, Norway, (2005).

[3] Deane, G.B. and Stokes, M.D. Scale dependence of bubble creation mechanisms in breaking waves. *Nature*, **418**, 839-844, (2002).

[4] Francois, M.M., Cummins, S.J., Dendy, E.D., Kothe, D.B., Sicilian, J.M. and Williams, M.W. A balanced-force algoritthm for continuous and sharp interfacial surface tension models within a volume tracking framework. *Journal of Computational Physics*, **213**, 141-173, (2006).

[5] Fedkiw, R.P., Aslam, T., Merriman, B. and Osher, S. A non-oscillatory Eulerian approach to interfaces in multimaterial flows (the ghost fluid method). *Journal of Computational Physics*, **152**, 457-492, (1999).

[6] Gerrits, J., Veldman, A.E.P. Dynamics of liquid-filled spacecraft. *Journal of Engineering Mathematics*, **45**, 21-38, (2003).

[7] Greco, M., Landrini, M. and Faltinsen, O.M. Impact flows and loads on ship-deck structures. *Journal of Fluids and Structures*, **19**, 251-275, (2004).

[8] Hao, Y. and Prosperetti, A. A numerical model for three-dimensional gas-liquid flow computations. *Journal of Computational Physics*, **196**, 126-144, (2004).

[9] Hirt, C.W., Nichols, B.D. Volume Of Fluid (VOF) Method for the Dynamics of Free Boundaries. *Journal of Computational Physics*, **39**, 201-225, (1981).

[10] Hu, C. and Kashiwagi, M. A CIP-based method for numerical simulations of violent free-surface flows. *Journal of Marine Science and Technology*, **9**, 143-157, (2004).

[11] Kleefsman, K.M.T., Fekken, G., Veldman, A.E.P., Buchner, B., Iwanowski, B. A Volume-Of-Fluid Based Simulation Method For Wave Impact problems. *Journal of Computational Physics*, **206**, 363-393, (2005).

[12] Peregrine, D.H. Water-wave impact on walls *Annual Review of Fluid Mechanics*, **35**, 23-43, (2003).

[13] Scardovelli, R., Zaleski, S. Direct Numerical Simulation of Free-Surface and Interfacial Flow. *Annual Review of Fluid Mechanics*, **31**, 567-603, (1999).

[14] Saurel, R. and Abgrall, R. A multiphase Godunov method for compressible multifluid and multiphase flows *Journal of Computational Physics*, **150**, 425-467, (1999).

[15] Tryggvason, G., Bunner, B., Esmaeeli, A., Juric, D., Al-Rawahi, N., Tauber, N., Han, J., Nas, S. and Jan, Y.J. A front-tracking method for the computations of multiphase flow *Journal of Computational Physics*, **169**, 708-759, (2001).

[16] Udaykumar, H.S., Kan, H., Shyy, W. and Tran-Son-Tay, R. Multiphase dynamics in arbitrary geometries on fixed cartesian grids. *Journal of Compuatational Physics*, **137**, 366-405, (1997).

[17] Wemmenhove, R., Loots, G.E., Luppes, R., Veldman, A.E.P. Modeling two-phase flow with offshore applications. *24th Offshore Mechanics and Arctic Engineering Conference, paper 67460*, Halkidiki, Greece, (2005).

[18] Yabe, T., Xiao, F., Utsumi, T. The constrained interpolation profile method for multiphase analysis. *Journal of Computational Physics*, **169**, 556-593, (2001).